The Structure and Energetics of Transient Disturbances in the Northern Hemisphere Wintertime Circulation[1]

NGAR-CHEUNG LAU[2]

Department of Atmospheric Sciences, University of Washington, Seattle 98195

(Manuscript received 3 November 1978, in final form 27 February 1979)

ABSTRACT

The hemispheric distributions of wintertime circulation statistics derived from the forecast fields of vertical motion are presented. The dominant features in the pattern for time-mean vertical velocity are consistent with the existence of thermally direct meridional circulations over the entrance regions of the principal jet streams, and thermally indirect circulations over the jet exit regions. Rising motions in the transient disturbances are seen to display positive temporal correlations with temperature and geopotential height over the major oceanic storm track regions. On the other hand, the western portion of the continents and the adjacent oceanic areas are characterized by downward eddy transports of geopotential energy at 850 and 500 mb, as well as much reduced temporal correlations between the vertical motion and temperature fields.

The vertical phase structure of the transient disturbances at various geographical locations is studied by performing a cross-spectral analysis of the time series of geopotential height fields at 850, 500 and 250 mb. The local geopotential height fluctuations at different pressure levels are strongly coherent. Over the sites characterized by enhanced development of transient waves, geopotential height perturbations of synoptic temporal scales are seen to lag by about 60° (1/6 cycle) between the tropopause and 850 mb levels. The corresponding phase lag is reduced to about 25° over the western portion of the continents, and the disturbances acquire a barotropic character at these longitudes.

The results of a detailed diagnosis of the local, time-averaged budgets of time-mean and transient eddy kinetic energy at 300 mb are discussed. The kinetic energy of the intensified time-mean flow at the jet stream cores is primarily maintained by the local, time-averaged ageostrophic circulations, which dominate over the effects due to eddy-mean flow interactions. The energy generated in these source regions is transported by the time-mean flow to the jet exit regions, where the thermally indirect circulations function as local sinks of mean kinetic energy. Analogously, eddy kinetic energy at the jet stream level is generated by ageostrophic motions in the transient disturbances over the western oceans, it is then advected to the western portion of the continents by the time-averaged flow, and is eventually dissipated by the supergeostrophic flow in the eddies at those longitudes.

The regional character of the transient eddy statistics presented in this and earlier papers is interpreted in the light of the results from a recent modeling study by Simmons and Hoskins (1978) on the life cycle of nonlinear baroclinic waves.

1. Introduction

The three-dimensional structure of the observed tropospheric circulation statistics for the Northern Hemisphere during the winter season has been investigated recently by Blackmon *et al.*, (1977, hereafter referred to as B) and Lau (1978, hereafter referred to as L). In these studies, the temporal mean, variance and covariance fields were documented using twice-daily hemispheric analyses of geopotential height, temperature and horizontal wind components for 11 individual winters. It was noted that the regional features of these statistics bear a definite relation to the distribution of continents and oceans. The western and central portions of the midlatitude oceans, which exhibit strong temporal fluctuations in the selected meteorological variables, are seen to be favored sites for baroclinic wave activity. Synoptic-scale disturbances associated with these "storm tracks" are characterized by strong poleward heat transports in the lower troposphere (B, Fig. 11b) and by strong momentum flux convergence at the upper levels (B, Fig. 7b). On the other hand, the meridional sectors corresponding to the western portion of the North American and Eurasian land masses, which lie to the east of these centers of activity, display quite different dynamical features. For example, the vertically integrated meridional eddy heat transports are weak (L, Figs. 9e and 9f) and the ageostrophic wind components in the eddies act to

[1] Contribution No. 484, Department of Atmospheric Sciences, University of Washington.

[2] Present affiliation: Geophysical Fluid Dynamics Program, Princeton University, Princeton, N.J. 08540.

0022-4928/79/060982-14$07.50

© 1979 American Meteorological Society

destroy eddy kinetic energy in the upper troposphere (L, Fig. 20).

In order to obtain a better understanding of these interesting longitudinal variations in the structure and energetics of the transient eddies, the previous analyses by B and L are extended in the present paper by examining 1) the hemispheric distributions of general circulation statistics involving large-scale vertical motions, 2) the geographical distribution of the vertical structure of transient disturbances at the frequencies associated with baroclinic wave activity, and 3) the local, time-averaged budgets of time mean and transient eddy kinetic energy. The information thus obtained will not only provide useful insights into energy transformation processes associated with transient and stationary motions at various geographical locations, but will also complement the earlier papers B and L in offering a three-dimensional description and interpretation of the wintertime circulation in the troposphere and lower stratosphere.

The synoptic-scale vertical velocity plays an important role in our understanding of the atmospheric circulation, and yet it has been one of the most difficult meteorological variables to determine with any precision. Wiin-Nielsen (1959, 1964) has demonstrated that plausible estimates of the conversion term between available potential and kinetic energy can be obtained by computing the vertical velocity as a by-product from a quasi-geostrophic numerical weather prediction model. Jensen (1961) and Molla and Loisel (1962) presented zonally-averaged statistics on the vertical transport processes over the Northern Hemisphere by making use of vertical motions deduced from the thermodynamic energy equation, neglecting diabatic heating. Oort and Peixóto (1974) studied the large-scale energetics of the Northern Hemisphere by computing the mean vertical velocity through vertical integration of the mass continuity equation.

The hemispheric vertical motion fields used in the present study are produced by the U.S. National Meteorological Center (NMC) forecast models. The length of the data records and the hemispheric coverage of these fields are such that we are able to present the statistics involving vertical motions in a format which is compatible with that of the earlier papers in this series of observational studies. Furthermore, since the same prediction models have been used to generate the forecast field of vertical motion and the first-guess fields for objective analyses of other meteorological variables (e.g., geopotential height, temperature, etc.), there should exist a strong degree of internal consistency between the vertical motion statistics obtained in this study and the results in B and L.

A brief description of the data base and the NMC forecast models used in computing the vertical motion field is given in Section 2 of this paper. The hemispheric distributions of the mean 500 mb vertical velocity and its temporal variability are presented in Section 3. The statistics on the vertical transports of geopotential energy and heat are discussed in Section 4. The results of a cross-spectral analysis of the geopotential height time series at various levels are presented, and the inferred vertical structures of the transient disturbances at various locations are discussed in Section 5. In Section 6 is shown the distribution of principal terms in the local, time-averaged budgets of time mean and transient eddy kinetic energy. In the concluding section, the regional characteristics of the transient eddies noted in L and the present paper are interpreted by comparing these observational results with those of a recent modeling study by Simmons and Hoskins (1978) on the life cycle of nonlinear baroclinic waves on a sphere.

2. Description of the data set

The data base for the present study consists of the twice-daily NMC analyses of the geopotential height, temperature and horizontal wind fields for 11 individual winters (1965–76) at selected pressure levels; as well as the corresponding 6 h forecast fields of vertical motion. The winter season is taken to be the 120-day period starting from 15 November. All variance and covariance statistics used in the present paper are computed with the unfiltered time series of atmospheric variables.

The data for vertical motions are available for the periods from 1964 to 1972, and from 1975 to 1977. During the six winters from 1966 to 1972, which constitute a major portion of these data records, the operational forecast procedure at NMC consisted of a daily analysis/forecast cycle. The two numerical weather prediction models used in this cycle are the 6-layer primitive equation model (usually in operation at 0000 GMT) and the 3-layer baroclinic model (usually in operation at 1200 GMT). The former model was described by Shuman and Hovermale (1968). It integrates directly the hydrostatic primitive equations at six prediction levels in the vertical. It employs a modified sigma-coordinate system consisting of four domains: a single planetary boundary layer, a 3-layer troposphere, a 2-layer stratosphere and a computational isentropic layer at the top. The earth's surface as well as the boundaries between the isentropic, stratospheric and tropospheric domains in this model are treated as material surfaces at which no mass exchange takes place. By making use of this assumption, the forecast fields of vertical motion are determined diagnostically from the mass continuity equation after 6 h of model integration. The 3-layer baroclinic model integrates a refined version of the prognostic equation for potential vorticity at the 850, 500 and 200 mb levels. The most essential departures of this model from its earlier prototypes are the inclusion of the divergent component of the wind field in the vorticity advection terms, and the use of the balance equation to preserve the relation-

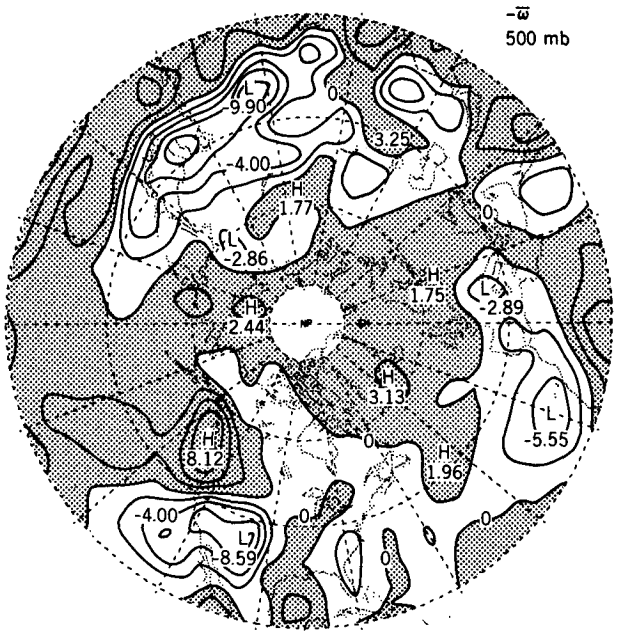

FIG. 1. Distribution of mean 500 mb pressure velocity, $-\bar{\omega}$, averaged over 11 winters. Contour interval 2×10^{-4} mb s^{-1}. For conversion from ω to vertical velocity w at 500 mb in mid-latitudes, multiply ω in units of 10^{-4} mb s^{-1} by 0.15 to obtain w in units of cm s^{-1}. Shading indicates rising motion. The meridians and latitude circles in this and the following figures are drawn at an interval of 20°. The outermost circle represents 20°N.

ship between the mass field and the wind field during the prediction. The 6 h forecast fields of vertical motion in this model are obtained by solving the omega equation.

3. The 500 mb vertical velocity field

The distribution of the time-averaged vertical velocity at 500 mb is shown in Fig. 1. In view of the fact that two different prediction models were used alternately at 0000 and 1200 GMT during most of the period from 1966 to 1972, and that some model changes probably occurred during this period, one might question the homogeneity of the data that made up this time average. In order to answer this question, we have partitioned the 500 mb vertical velocity data for this period into four different categories: 1966–69 (0000 and 1200 GMT), 1969–72 (0000 and 1200 GMT), 1966–72 (0000 GMT) and 1966–72 (1200 GMT). The hemispheric fields obtained by averaging the data in each of these four subsets (not shown) display a strong resemblance to the long-term average distribution presented in Fig. 1. The forecast fields of vertical motion are hence seen to be rather independent of the particular model version used.

It is seen from Fig. 1 that the eastern portion of the Asian continent is dominated by mean rising motion over the warm maritime regions in the subtropics, and mean sinking motion over the cold continental regions in higher latitudes. The North American continent is dominated by strong ascent along the North Pacific coast; and by subsidence over the southwestern United States, which extends westward off the coast of Southern California. Weak subsidence prevails over the eastern seaboard of the United States and the adjacent regions of the western Atlantic. Weak ascent covers northern Europe, while subsidence prevails over the Mediterranean, north Africa and the subtropical eastern Atlantic. With the exception of the rising motion at 20°N over the Sahara, the major features in Fig. 1 are consistent with the hemispheric distribution of mean precipitation estimated by Möller (1951) and reproduced by Manabe and Holloway (1975, Fig. 13), the mean cloud coverage patterns deduced from meteorological satellite measurements (U.S. Dept. of Commerce and U.S. Air Force, 1971, p. 106), and the vertical velocity field produced by a general circulation model developed at the Geophysical Fluid Dynamics Laboratory (Manabe and Holloway, 1975, Fig. 5).

The dipole-like structure in the time-averaged vertical motion field over eastern Asia (i.e., ascent over regions south of 30°N and subsidence over regions further north) is indicative of the presence of poleward cross-isobar flow in the entrance region of the Asian jet stream. This is in agreement with the heuristic models for the maintenance of the jet streams, as proposed by Namias and Clapp (1949) and B. On the other hand, the jet exit regions over eastern oceans are characterized by sinking over the subtropics and rising motion at higher latitudes. This suggests that equator-

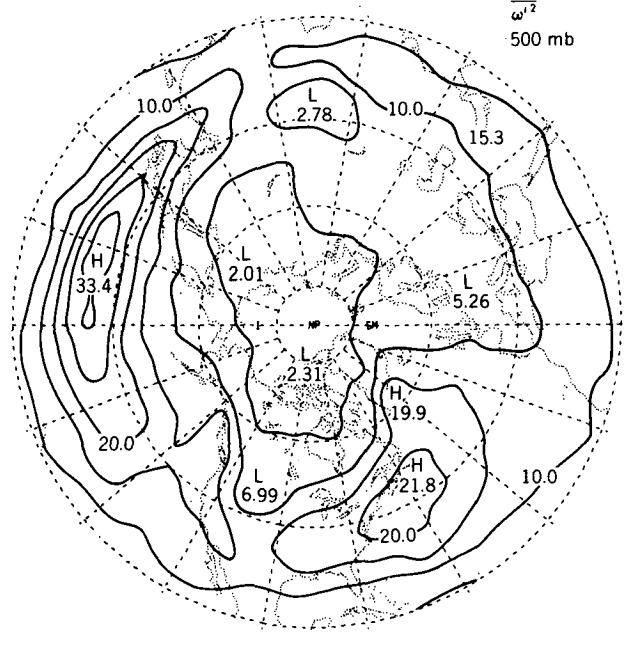

FIG. 2. Distribution of the temporal variance of pressure velocity, $\overline{\omega'^2}$, at 500 mb. Contour interval 5×10^{-7} mb^2 s^{-2}.

ward cross-isobar flow prevails in the upper troposphere at these longitudes.

In Fig. 2 is shown the distribution of the temporal variance of the 500 mb vertical velocity. This field is seen to exhibit elongated maxima over the western part of the midlatitude oceans. Except for a slight equatorward shift of the maximum over the Pacific, the locations of these maxima coincide closely with the major storm tracks, where strong fluctuations of geopotential height, temperature and the meridional wind component with synoptic (2.5–6 days) time scales are noted in B. In contrast to these active regions, the western part of the North American and Eurasian land masses as well as central Asia are seen to be characterized by very low variability in the vertical motion field.

4. Vertical transports by the transient eddies

The geographical distribution of the vertical transport of geopotential energy by the transient eddies through the 850, 500 and 300 mb surfaces are presented in Fig. 3. Over the oceanic storm track regions, the transient eddies transport geopotential energy upward at all three levels. The intensity of these fluxes increases by almost an order of magnitude between the 850 mb level and the tropopause. On the other hand, the western portion of the continents and central Asia are characterized by downward geopotential energy fluxes in the lower troposphere, and very weak transports in the upper troposphere.

In Fig. 4 is shown the distribution of the vertical transport of heat by transient eddies at 700 mb. The positive maxima over the principal storm tracks and the Gulf of Alaska indicate a strong tendency for ascent of warm air and subsidence of cold air in the

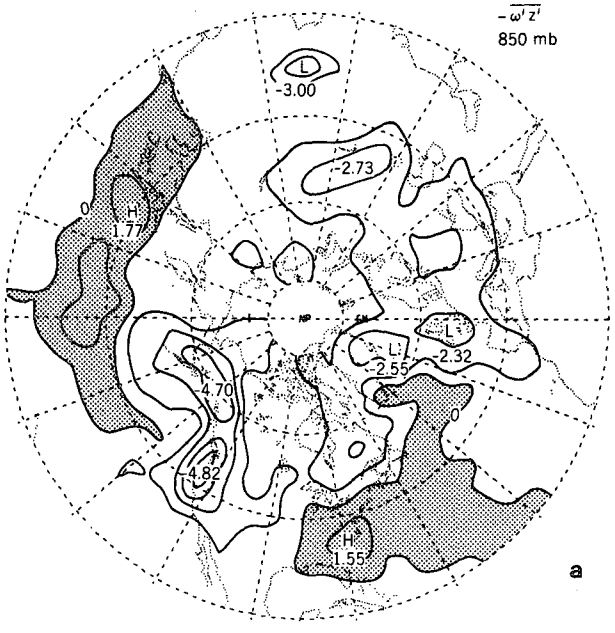

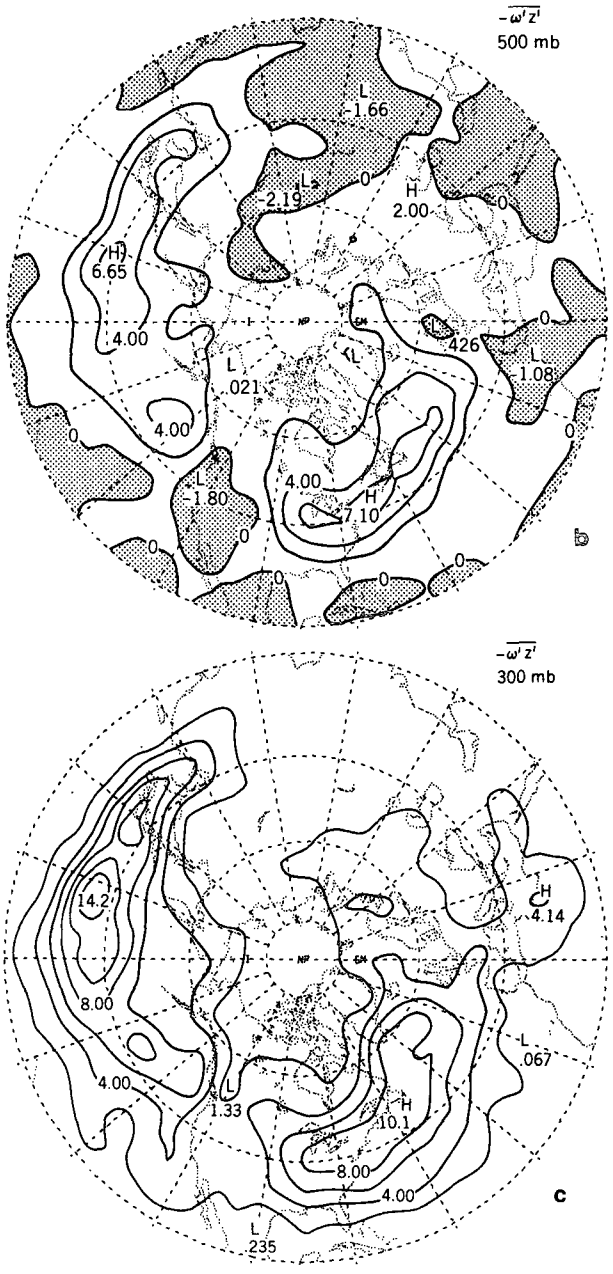

FIG. 3. Distributions of the vertical transport of geopotential energy by transient eddies, $-\overline{\omega'z'}$, at (a) 850 mb, contour interval 1×10^{-2} m mb s^{-1}, shading indicates upward transport; (b) 500 mb, contour interval 2×10^{-2} m mb s^{-1}, shading indicates downward transport; and (c) 300 mb, contour interval 2×10^{-2} m mb s^{-1}.

eddies over these active regions. The temporal fluctuations of vertical motion and temperature over the western continents are characterized by weak and, in some cases, slightly negative correlations.

5. Vertical structure of the transient disturbances

The striking longitudinal variations in the circulation statistics presented in B, L and the present paper

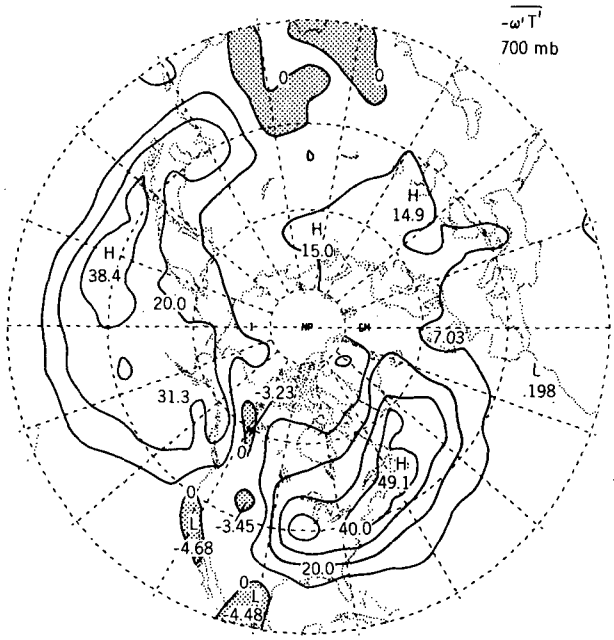

FIG. 4. Distribution of the vertical transport of heat by transient eddies, $-\overline{\omega' T'}$, at 700 mb. Contour interval 1×10^{-3} °C mb s^{-1}.

suggest that the transient disturbances in various regions are characterized by quite different structures and energetics. In order to obtain a better understanding of the regional variations in the vertical structure of these transient eddies, we have performed a cross-spectral analysis of the time series of the geopotential height fields at the 850, 500 and 250 mb levels, so as to establish vertical phase relationships at different locations. The data for 1000 mb are not included in this analysis in view of the uncertainties inherent in the sea level pressure corrections over regions of high terrain. At each point in a 10°×10° latitude-longitude grid, the power spectra for individual pressure levels, as well as the quadrature spectra and cospectra for pairs of pressure levels, were computed using the lag-correlation method. The calculations were performed using 20 lags, so that each cross-spectral estimate has a bandwidth of (1/20) day^{-1}.

The hemispheric distribution of the vertical phase relationships in transient disturbances with periods between about 4.5 to 6 days is displayed in Fig. 5, for phase differences between the 850 and 500 mb levels (Fig. 5a), and the 500 and 250 mb levels (Fig. 5b). The orientation of each arrow in this figure depicts the phase difference between the pair of pressure levels at that particular grid point. An arrow pointing from south to north indicates zero phase difference, one pointing from west to east indicates that the geopotential height fluctuations at the upper level lag the corresponding fluctuations at the lower level by $\frac{1}{8}$ cycle (45°), and one pointing from north to south indicates a phase lag of $\frac{1}{4}$ cycle (90°), etc. (i.e., if the fluctuations at the upper level lag the fluctuations at the lower level, the arrows rotate clockwise 2° per each degree of phase lag).[3] The coherence of the pair of time series, which provides for an objective statistical measure of the reliability of the phase relationships, is indicated by the length of the arrows according to the scale at the lower left of the figure. For the 10-winter data record totaling 2400 data points, a conservative estimate of the number of degrees of freedom corresponding to 20 lags is given by 2400/20=120, so that the limiting coherence at the 99.9% significance level is approximately 0.25 (Amos and Koopmans, 1963). Examination of Fig. 5 reveals that, except for the few grid points over eastern China, the values of the coherence are typically above 0.7, which is well above the 99.9% significance level. Hence the phase structure deduced in this analysis should be quite reliable. Over the western Pacific and eastern United States, where the transient disturbances are actively growing, the geopotential height fluctuations at the 500 mb level are seen to lag those at the 850 mb level by about 45°, while the fluctuations at 250 mb lag by another 15°. As we move eastward across the major oceans and reach the west coasts of the North American and European continents, where the level of eddy activities is much weakened, we notice a remarkable reduction in the phase lag with height. The phase difference over the eastern oceans is generally about 15° between 850 and 500 mb, and less than 10° between 500 and 250 mb. The vertical phase structure over the mid-Atlantic is in good agreement with the results of Hartmann (1974), who performed a similar analysis of rawinsonde observations from two weather ships located in that region.

Another remarkable feature in Fig. 5a is the occurrence of rather strong phase lags over the Siberian region located between 80°E and 120°E, and centered at 50°N. This region corresponds closely to maxima in the variance of geopotential height (Blackmon, 1976, Fig. 3a) and poleward momentum transport by the transient eddies (Lau *et al.*, 1978, Fig. 1a).

It is interesting to note that the phase lag between 850 and 500 mb (Fig. 5a) is largest over regions lying east of the Rockies and Himalayas. The phase lag over the same regions is much reduced in the upper troposphere (Fig. 5b). This indicates that the synoptic systems over the lee slopes of major mountain barriers are shallow and highly baroclinic, in agreement with the discussion in B (Section 8b).

In Fig. 6 is shown the distribution of the phase difference between 850 and 500 mb for more slowly varying disturbances with periods between about 8–13 days. The phase lag between these two levels

[3] If the geopotential height fluctuations at the lower level lag the corresponding fluctuations at the upper level, the arrows rotate *counterclockwise* 2° per each degree of phase lag. Since the maximum observed phase lag in either sense does not exceed 90°, the phase convention adopted here does not lead to any ambiguities.

decreases from about 20° over the storm track regions to almost 0° over the eastern oceans. Also notable are the large phase lags over the Siberian region mentioned earlier. The corresponding distribution of the phase difference between 500 and 250 mb (not shown) is characterized by very small lags at most locations, ranging from 10° over the western oceans to near zero over the western continents.

Since most of the midlatitude geopotential height variance within synoptic time scales is accounted for by eastward propagating disturbances (e.g., see Pratt and Wallace, 1976, Fig. 1), a phase lag in time with increasing height may be interpreted as a westward tilt in space. The results of this cross-spectrum analysis hence may be summarized and integrated with the observed transient eddy statistics in the idealized structures of the disturbances shown in Fig. 7. Over the active regions in the vicinity of the oceanic storm tracks (Fig. 7a), the synoptic-scale disturbances have a structure characteristic of a developing baroclinic wave (Wallace and Hobbs, 1977, Fig. 9.13). The westward tilt of the wave axes with increasing height is particularly marked in the lower troposphere. At these levels the temperature wave lags the pressure wave by about one-quarter wavelength, in agreement with the strong positive correlation between meridional motion and temperature fluctuations observed in B (Fig. 11b). The ageostrophic flow in the disturbance acts to generate eddy kinetic energy at the jet stream level, in agreement with the result in L (Fig. 20). Associated with this cross-isobar flow pattern is a thermally direct circulation with positive correlations between rising motion and positive temperature anomalies, as indicated in Fig. 4 of this paper. The in-phase relationship between vertical motion and geopotential fluctuations in the upper troposphere are indicative of strong upward fluxes of geopotential energy near the tropopause (Fig. 3c). It is also evident that the vertical and meridional motions in the developing waves are positively correlated in the middle troposphere.

Over the western portion of the major land masses and the adjacent oceanic areas (Fig. 7b), the transient disturbances acquire a more barotropic character, with much reduced tilt of the wave axes with altitude. The tendency for the cross-isobar flow to be directed from low to high pressure in the upper troposphere is consistent with the observed destruction of kinetic energy at these levels (L, Fig. 20). This ageostrophic flow pattern drives a circulation characterized by downward transport of geopotential energy in the middle and lower troposphere, as indicated in Figs. 3a and 3b.

6. The time-averaged kinetic energy budgets

In order to investigate how the local kinetic energy balances are affected by regional differences in the structure of the transient disturbances, and to evaluate the relative importance of various types of interactions between the eddies and the time mean flow, it is useful to consider the time-averaged budgets of time mean and transient eddy kinetic energy. The data for 300 mb are used in this analysis, since this pressure level corresponds to maximum eddy kinetic energy.

The balance for the kinetic energy of the time averaged flow may be expressed as

$$
\begin{aligned}
\frac{\partial}{\partial t}\bar{K}_M = & -\frac{1}{a\cos\phi}\left(\frac{\partial}{\partial\lambda}\bar{u}\bar{K}_M+\frac{\partial}{\partial\phi}\bar{v}\bar{K}_M\cos\phi\right)-\frac{\partial}{\partial p}\bar{\omega}\bar{K}_M && \Big\}\ \text{A}\\
& -\bar{u}\left[\frac{1}{a\cos\phi}\left(\frac{\partial}{\partial\lambda}\overline{u'u'}+\frac{\partial}{\partial\phi}\overline{v'u'}\cos\phi\right)+\frac{\partial}{\partial p}\overline{\omega'u'}-\frac{\tan\phi}{a}\overline{u'v'}\right] && \Big\}\ \text{B}\\
& -\bar{v}\left[\frac{1}{a\cos\phi}\left(\frac{\partial}{\partial\lambda}\overline{u'v'}+\frac{\partial}{\partial\phi}\overline{v'v'}\cos\phi\right)+\frac{\partial}{\partial p}\overline{\omega'v'}+\frac{\tan\phi}{a}\overline{u'u'}\right] && \Big\}\ \text{B}\\
& +f(\bar{u}\bar{v}_a-\bar{v}\bar{u}_a) && \Big\}\ \text{C}\\
& +\bar{u}\bar{F}_\lambda+\bar{v}\bar{F}_\phi && \Big\}\ \text{D}
\end{aligned}
\qquad (1)
$$

where overbars denote time averages, primes represent deviations from the corresponding time averaged quantities, the subscript a refers to ageostrophic wind components, λ is longitude, ϕ latitude, a earth radius, p pressure, F_λ, F_ϕ are components of frictional and sub-grid scale dissipation, $\bar{K}_M=\frac{1}{2}(\bar{u}^2+\bar{v}^2)$ is the kinetic energy of the time-averaged flow, and all other symbols are used in their conventional meteorological context.

The first triad of terms A represents the local convergence of $\bar{K}_M$ due to transport of this quantity by the time mean flow. The second group of terms B represents the contribution of transient eddy fluxes to the maintenance of the time mean flow. The term C represents effects of the local time averaged ageostrophic flow in the generation or destruction of $\bar{K}_M$. Finally, the dissipation through work done by viscous forces is given by term D.

The ageostrophic wind components in the term

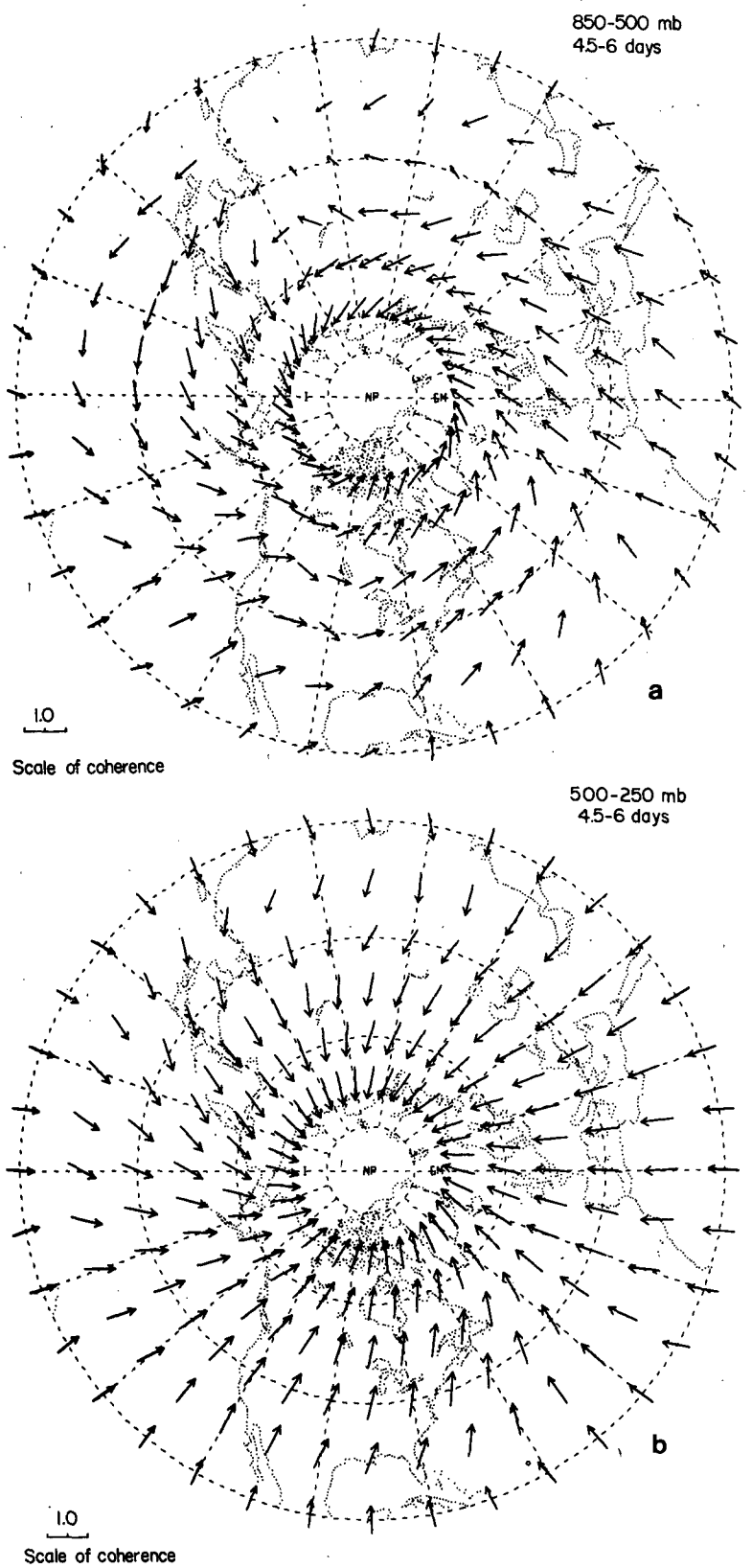

FIG. 5. Distributions of the phase lag in transient disturbances with periods of 4.5–6 days, between (a) the 850 and 500 mb levels and (b) the 500 and 250 mb levels. An arrow pointing from south to north indicates zero phase difference, one

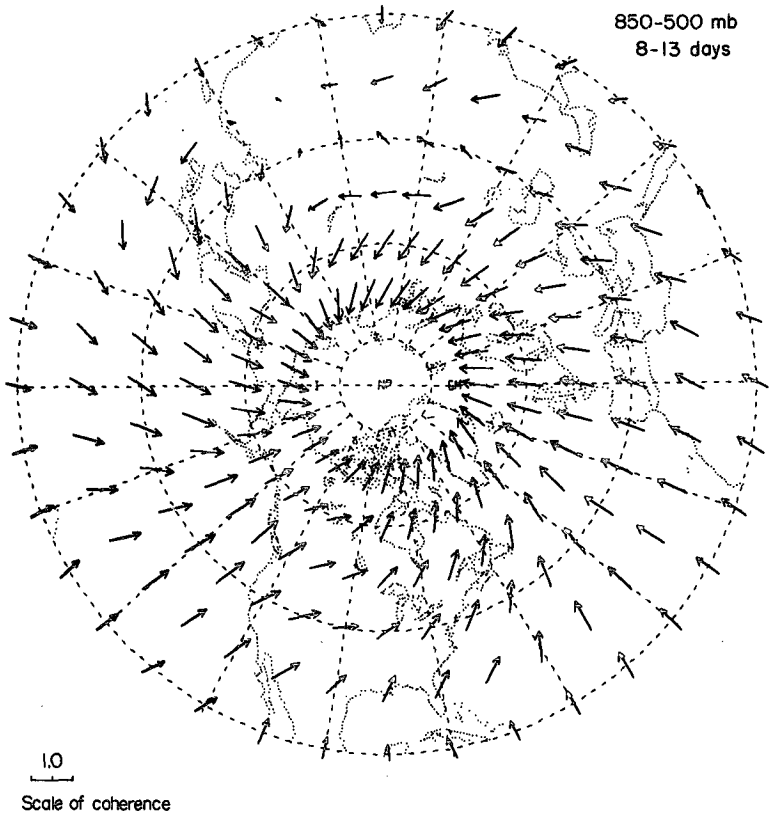

FIG. 6. As in Fig. 5a, but for geopotential height fluctuations within the 8–13 day period range.

$f(\bar{u}\bar{v}_a-\bar{v}\bar{u}_a)$ may be computed by the two methods discussed in Section 6 of L. With the direct method, the ageostrophic winds are obtained by subtracting the geostrophic wind components from the NMC analyzed wind data. The indirect method makes use of the time-averaged momentum equations, from which the departure of the wind field from geostrophy may be estimated as a residue. The distributions of term C, as computed by the direct and indirect methods, are shown in Figs. 8a and 8b, respectively. The estimate of the ageostrophic term by the indirect method is seen to be larger than that by the direct method. This may be a consequence of the inherent bias in the NMC analysis procedures toward gradient wind balance, which results in underestimation of the cross-isobar flow. Despite this discrepancy, there exists a strong correspondence between these two distributions with respect to the locations of the principal maxima and minima.

Since we generally have $\bar{u}\bar{v}_a>\bar{v}\bar{u}_a$ and $\bar{u}>0$, the distribution of $f(\bar{u}\bar{v}_a-\bar{v}\bar{u}_a)$ is primarily determined by the longitudinal variation of the time-averaged, meridional ageostrophic flow $\bar{v}_a$. It is seen from Fig. 8 that the poleward ageostrophic flows over the jet entrance regions (eastern Asia and eastern United States) result in large local generations of $\bar{K}_M$, while the equatorward ageostrophic flows accompanying the thermally indirect circulations over the oceanic regions lead to destruction of $\bar{K}_M$. These results are consistent with those presented by Oort and Chan (1977, Fig. 6) on the longitudinal variation of poleward momentum transport across the 27.5°N latitude circle.

In Fig. 9 is shown the distribution of the local convergence of $\bar{K}_M$ due to transport by the horizontal

pointing from west to east indicates that the geopotential height at the upper level lags the corresponding fluctuations at the lower level by 1/8 cycle (45°), and one pointing from north to south indicates a phase lag of 1/4 cycle (90°), etc. (i.e., if the fluctuations at the upper level lag the fluctuations at the lower level, the arrows rotate clockwise 2° per each degree of phase lag). The coherence is indicated by the length of the arrows according to the scale at the lower left of the figure.

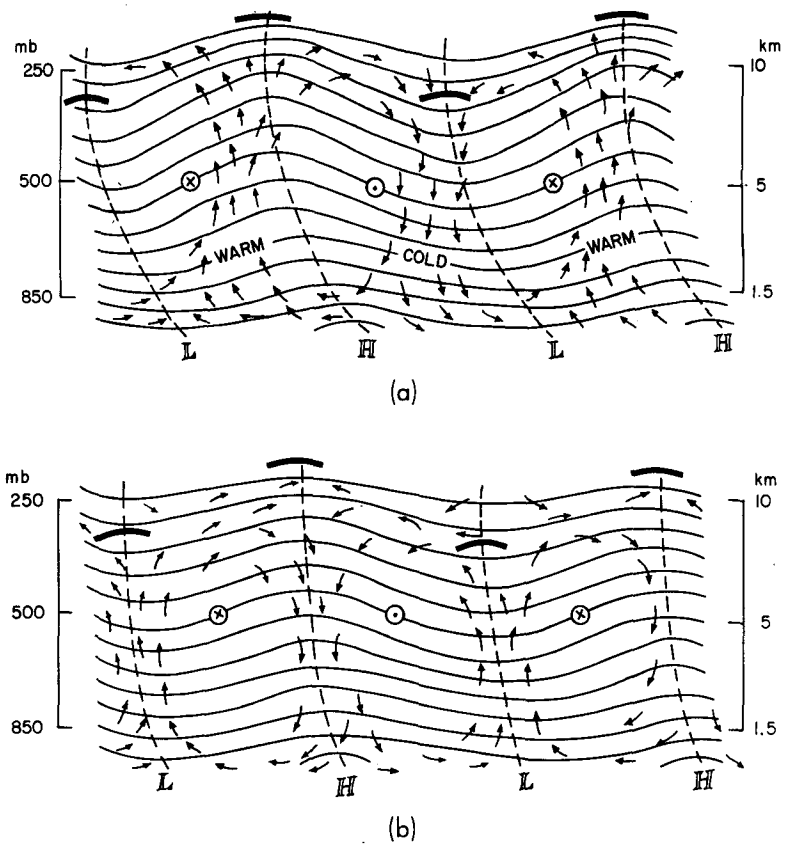

FIG. 7. Idealized structure of the circulation in the zonal plane in typical disturbances over (a) the oceanic storm tracks and (b) the western continents. Solid lines represent pressure surfaces. Dashed lines show the vertical tilt of the wave axis in the geopotential height field. Heavy lines indicate the position of the tropopause. Arrows denote vertical motions and the associated cross-isobar flow. Crosses and dots indicate poleward and equatorward geostrophic motions, respectively. Fig. 7a is adapted from Wallace and Hobbs (1977, Fig. 9.13).

time-averaged flow (term A).[4] The time-mean flow is seen to transport $\bar{K}_M$ from the jet stream cores (where $\bar{K}_M$ is maximum) to the adjacent oceanic areas.

In Fig. 10 is shown the distribution of term B. Since $\overline{u'u'} \approx \overline{v'v'} \gg \overline{u'v'}$, this group of terms is dominated by the components

$$-\frac{\bar{u}}{a\cos\phi}\frac{\partial}{\partial\lambda}\overline{u'u'} \quad \text{and} \quad -\frac{\bar{v}}{a\cos\phi}\frac{\partial}{\partial\phi}\overline{v'v'}\cos\phi.$$

[4] The terms in (1) that involve vertical motions are not considered in the present analysis because they should be of order Rossby number (~0.15) times the terms that involve horizontal motions. It should be noted that, after neglecting effects of vertical motions, terms A in (1) may be written as $-\nabla\cdot\bar{\mathbf{V}}\bar{K}_M = -\bar{\mathbf{V}}\cdot\nabla\bar{K}_M - \bar{K}_M\nabla\cdot\bar{\mathbf{V}}$, where ∇ is the horizontal gradient operator. Comparison between the local magnitudes of the terms $\bar{\mathbf{V}}\cdot\nabla\bar{K}_M$ and $\bar{K}_M\nabla\cdot\bar{\mathbf{V}}$ (not shown) using NMC data indicates that $\bar{\mathbf{V}}\cdot\nabla\bar{K}_M \gg \bar{K}_M\nabla\cdot\bar{\mathbf{V}}$. Hence the distribution in Fig. 9 may also be interpreted as portraying the horizontal advection of $\bar{K}_M$ by the time mean flow. The same remarks also apply to the distribution of $-\nabla\cdot\bar{\mathbf{V}}\bar{K}_T$ to be shown in Fig. 12a.

The essential features of Fig. 10 may hence be explained by considering the mean streamline pattern in relation with the locations of the oceanic storm tracks, where $\overline{u'u'}$ and $\overline{v'v'}$ attain maximum values. It is readily seen from such considerations that the regions located to the west and south of the storm tracks are characterized by negative values, whereas positive values prevail over regions located to the east and north of these centers of activity. Comparison between the distributions in Figs. 9 and 10 indicates that term A is generally larger than term B by a factor of 2–4.

In the absence of friction and vertical motions, the cumulative contributions to the $\bar{K}_M$ budget by the terms depicted in Figs. 9 and 10 must be balanced by the local generation or destruction of $\bar{K}_M$ due to ageostrophic motions in the time-averaged flow (Fig. 8). Inspection of the distributions in these figures indicates that the local sources and sinks of $\bar{K}_M$ due to ageostrophic flows are primarily balanced by mean flow advection, which dominates over effects due to the presence of transient eddies.

The balance for the kinetic energy of the transient eddies may be expressed as

$$\frac{\partial}{\partial t}\bar{K}_T = -\frac{1}{a\cos\phi}\left(\frac{\partial}{\partial\lambda}\bar{u}\bar{K}_T + \frac{\partial}{\partial\phi}\bar{v}\bar{K}_T\cos\phi\right) - \frac{\partial}{\partial p}\bar{\omega}\bar{K}_T \quad \Big\} \text{A}$$

$$-\frac{1}{a\cos\phi}\left(\frac{\partial}{\partial\lambda}\overline{u'K_T} + \frac{\partial}{\partial\phi}\overline{v'K_T}\cos\phi\right) - \frac{\partial}{\partial p}\overline{\omega'K_T} \quad \Big\} \text{B}$$

$$-\frac{1}{a\cos\phi}\left(\overline{u'u'}\frac{\partial\bar{u}}{\partial\lambda} + \overline{u'v'}\frac{\partial\bar{v}}{\partial\lambda}\right) - \frac{1}{a}\left(\cos\phi\,\overline{v'u'}\frac{\partial}{\partial\phi}\frac{\bar{u}}{\cos\phi} + \overline{v'v'}\frac{\partial\bar{v}}{\partial\phi}\right) - \overline{\omega'u'}\frac{\partial\bar{u}}{\partial p} - \overline{\omega'v'}\frac{\partial\bar{v}}{\partial p} + \bar{v}\overline{u'u'}\frac{\tan\phi}{a} \quad \Big\} \text{C} \qquad (2)$$

$$+f(\overline{u'v_a'} - \overline{v'u_a'}) \quad \Big\} \text{D}$$

$$+\overline{u'F_\lambda'} + \overline{v'F_\phi'} \quad \Big\} \text{E}$$

where $\bar{K}_T = \frac{1}{2}(\overline{u'^2} + \overline{v'^2})$ is the transient eddy kinetic energy.

The term A refers to the local convergence of $\bar{K}_T$ due to transports by the stationary flow. The term B, which involves triple correlation statistics, represents the convergence of K_T due to transient eddy fluxes. The next group of terms C represents the exchange of kinetic energy between the eddies and the mean flow. The term D represents the local generation or destruction of $\bar{K}_T$ due to ageostrophic motions in the eddies, and term E represents viscous effects.

The hemispheric distribution of the quantity $f(\overline{u'v_a'} - \overline{v'u_a'})$ at 300 mb is shown in Fig. 11. Since the cross-isobar component of the NMC wind analyses is underestimated, it is anticipated that the actual magnitudes of the term D are substantially larger than those depicted in this figure. The ageostrophic motions in the transient disturbances are seen to generate $\bar{K}_T$ over the western oceans, whereas the western continents are characterized by kinetic energy destruction due to strong supergeostrophic flow in the eddies (L, Fig. 19). These observed features reflect the prevalent cross-isobar flows from high to low pressure over the storm track regions; and from low to high pressure over the western continents in the upper tropsophere, as described in Fig. 7. It is worth noting that the absolute magnitudes of the maxima and minima in the generation term for $\bar{K}_T$ in Fig. 11 are weaker than the corresponding magnitudes for $\bar{K}_M$ in Fig. 8a by a factor of about 3–4.

In Fig. 12 is shown the distributions of the convergence of $\bar{K}_T$ due to transports by (a) horizontal mean

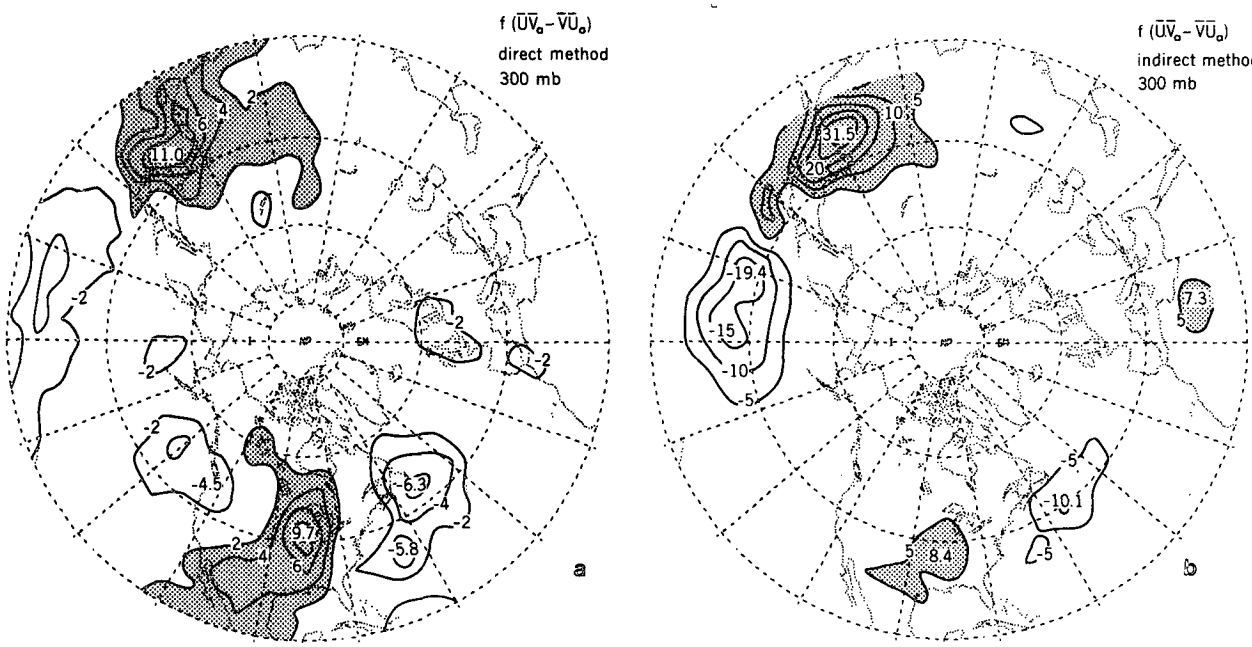

FIG. 8. Distributions of the term $f(\bar{u}\bar{v}_a - \bar{v}\bar{u}_a)$ at 300 mb, as computed by (a) the direct method, contour interval 2×10^{-3} m^2 s^{-3}, and (b) the indirect method, contour interval 5×10^{-3} m^2 s^{-3}. For the sake of clarity, the zero contour is not plotted.

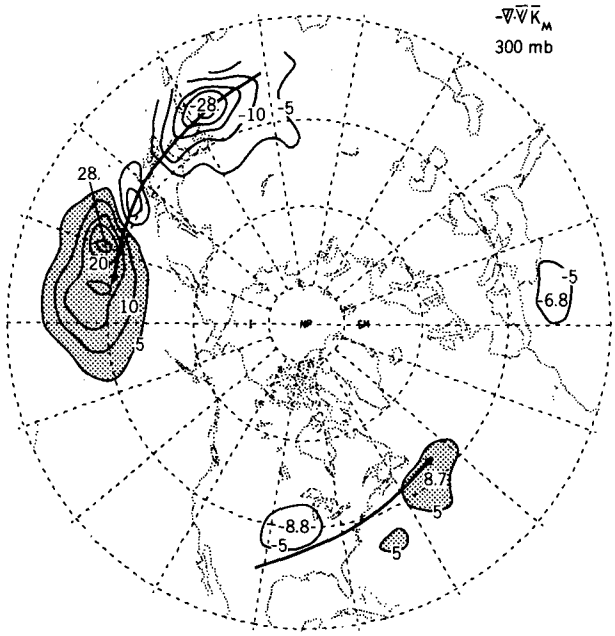

FIG. 9. Distribution of the term

$$-\frac{1}{a\cos\phi}\left(\frac{\partial}{\partial\lambda}\bar{u}\bar{K}_M+\frac{\partial}{\partial\phi}\bar{v}\bar{K}_M\cos\phi\right)$$

at 300 mb. Contour interval 5×10^{-3} m^2 s^{-3}. For the sake of clarity, the zero contour is not plotted. Arrows denote locations of the jet streams.

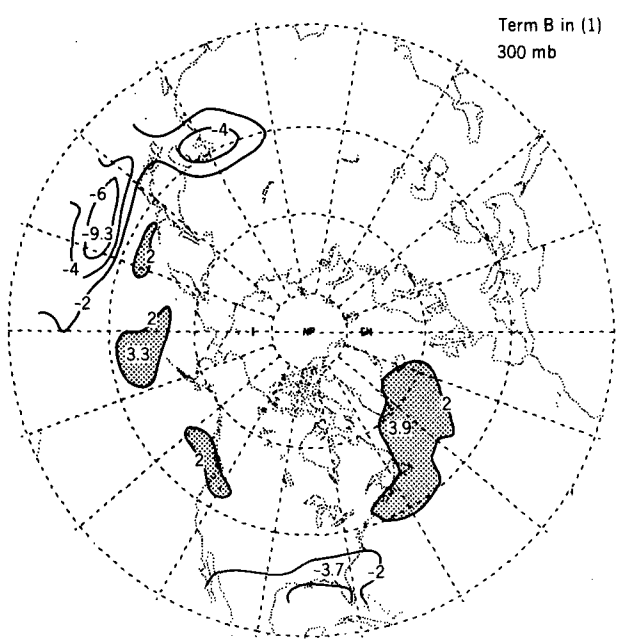

FIG. 10. Distribution of the term

$$-\bar{u}\left[\frac{1}{a\cos\phi}\left(\frac{\partial}{\partial\lambda}\overline{u'u'}+\frac{\partial}{\partial\phi}\overline{v'u'}\cos\phi\right)-\frac{\tan\phi}{a}\overline{u'v'}\right]$$

$$-\bar{v}\left[\frac{1}{a\cos\phi}\left(\frac{\partial}{\partial\lambda}\overline{u'v'}+\frac{\partial}{\partial\phi}\overline{v'v'}\cos\phi\right)+\frac{\tan\phi}{a}\overline{u'u'}\right]$$

at 300 mb. Contour interval 2×10^{-3} m^2 s^{-3}. For the sake of clarity, the zero contour is not plotted.

flow (term A), (b) horizontal transient motions (term B), and (c) by both mean and transient motions.[5] The overall patterns for both the mean flow and the eddies indicate the presence of flux divergence of $\bar{K}_T$ in the regions of activity over the oceanic storm tracks, and flux convergence over the western continents. Comparison between Figs. 12a and 12b reveals that the local convergence due to transport by the mean flow is generally larger than that by the transient eddies by a factor of about 2.

The distribution of the eddy-mean flow interaction term C is presented in Fig. 13. Comparison between this distribution and that of the flux convergence term in Fig. 12c suggests that the maxima in the absolute magnitude of the latter tend to be relatively larger by a factor of 2–3.

When the effects of viscous dissipation and terms involving vertical motion are neglected, the $\bar{K}_T$ budget requires a high degree of local compensation between the ageostrophic correlation term shown in Fig. 11, and the cumulative effects of flux convergence (Fig. 12c) and eddy-mean flow interactions (Fig. 13). Although the uncertainties of the ageostrophic correlation term prevent us from achieving an exact balance, comparison

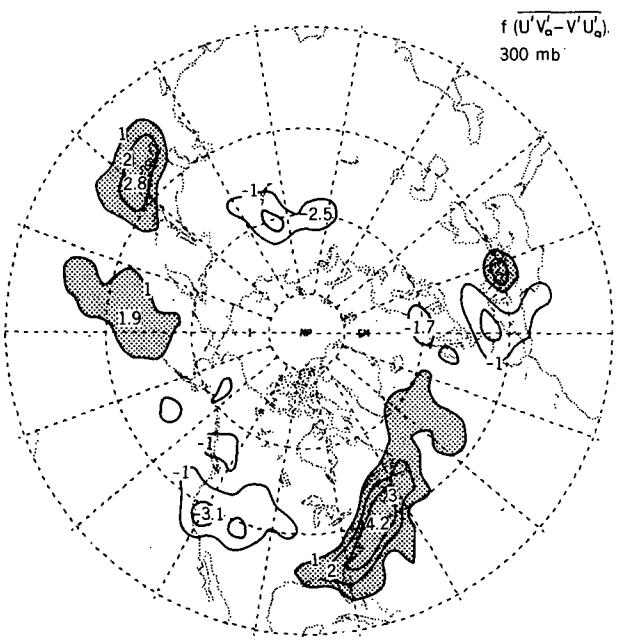

FIG. 11. Distribution of the term $f(\overline{u'v'_a}-\overline{v'u'_a})$ at 300 mb. Contour interval 1×10^{-3} m^2 s^{-3}. For the sake of clarity, the zero contour is not plotted.

[5] As was done in the diagnosis of the $\bar{K}_M$ budget, the terms in (2) which involve vertical motions are neglected. Also refer to footnote 4.

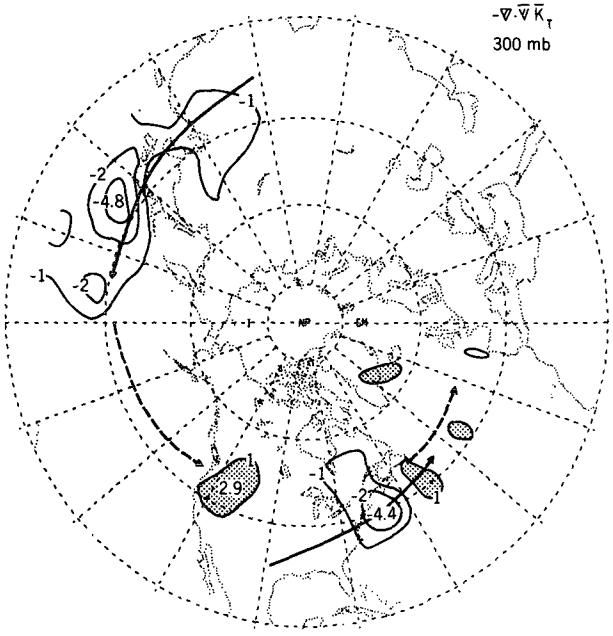

FIG. 12a. Distribution of the term

$$-\frac{1}{a\cos\phi}\left(\frac{\partial}{\partial\lambda}\bar{u}\bar{K}_T+\frac{\partial}{\partial\phi}\bar{v}\bar{K}_T\cos\phi\right)$$

at 300 mb. Contour interval 1×10^{-3} m^2 s^{-3}. For the sake of clarity, the zero contour is not plotted. Arrows with solid shafts denote locations of the jetstreams. Arrows with dashed shafts correspond to regions with maximum $\bar{K}_T$.

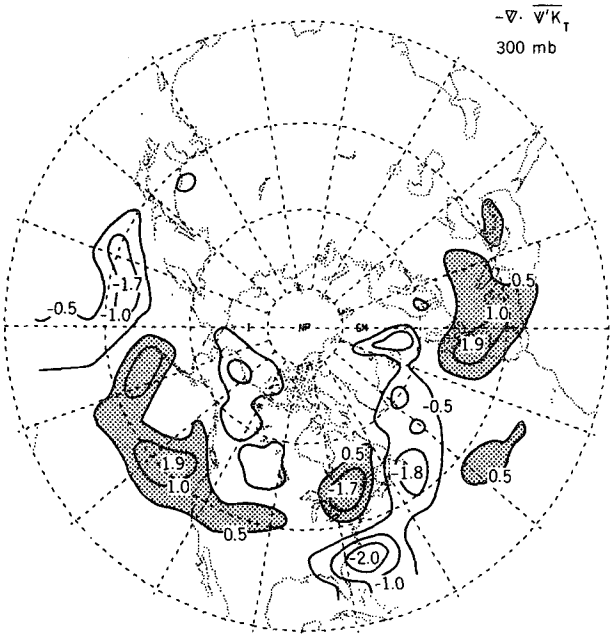

FIG. 12b. Distribution of the term

$$-\frac{1}{a\cos\phi}\left(\frac{\partial}{\partial\lambda}\overline{u'K_T}+\frac{\partial}{\partial\phi}\overline{v'K_T}\cos\phi\right)$$

at 300 mb. Contour interval 0.5×10^{-3} m^2 s^{-3}. For the sake of clarity, the zero contour is not plotted.

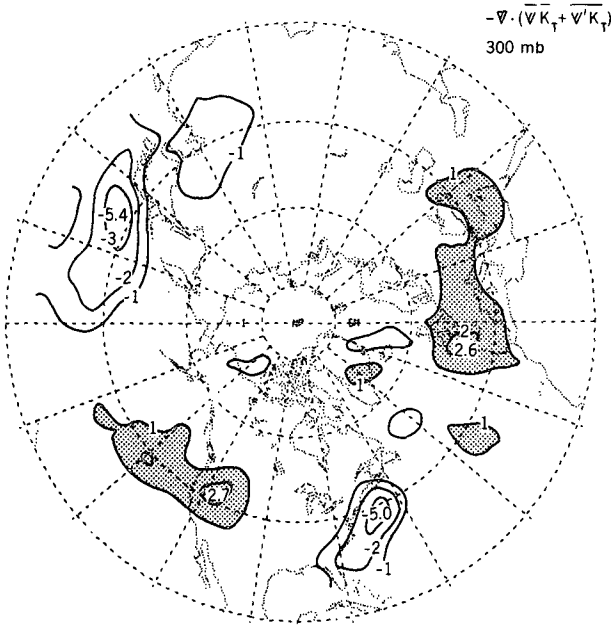

FIG. 12c. Distribution of the sum of the terms displayed in Figs. 12a and 12b. Contour interval 1×10^{-3} m^2 s^{-3}. For the sake of clarity, the zero contour is not plotted.

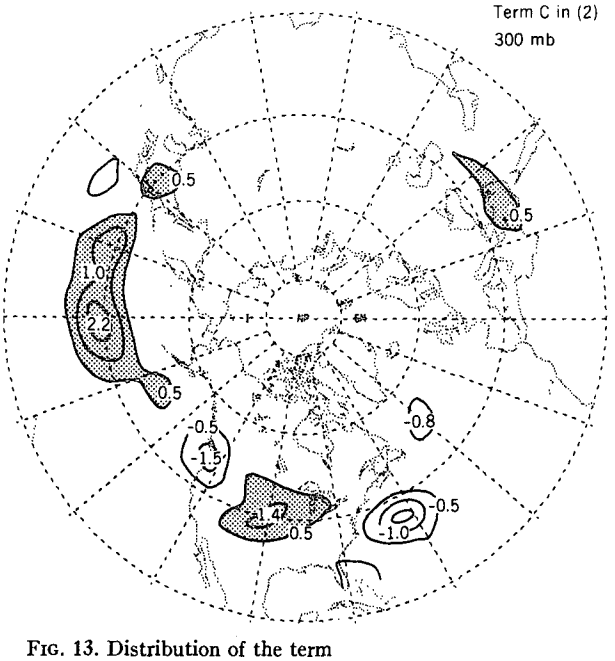

FIG. 13. Distribution of the term

$$-\frac{1}{a\cos\phi}\left(\overline{u'u'}\frac{\partial\bar{u}}{\partial\lambda}+\overline{u'v'}\frac{\partial\bar{v}}{\partial\lambda}\right)+\bar{v}\,\overline{u'u'}\frac{\tan\phi}{a}$$

$$-\frac{1}{a}\left(\cos\phi\overline{v'u'}\frac{\partial}{\partial\phi}\frac{\bar{u}}{\cos\phi}+\overline{v'v'}\frac{\partial\bar{v}}{\partial\phi}\right)$$

at 300 mb. Contour interval 0.5×10^{-3} m^2 s^{-3}. For the sake of clarity, the zero contour is not plotted.

of the distributions of the terms in (2) does identify the primary sources and sinks of $\bar{K}_T$ and the regional characteristics of the physical processes involved. Specifically, the ageostrophic motions in the transient disturbances act to generate $\bar{K}_T$ over the western oceans, whereas ageostrophic effects over the western continents bring about local destruction of eddy kinetic energy. The principal mechanism counterbalancing these local generation and destruction processes is the flux convergence due to the transport of $\bar{K}_T$ by the time mean flow (Fig. 12a), which dominates over the effects associated with transport by the transient motions (Fig. 12b) and eddy-mean flow interactions (Fig. 13).

A similar diagnosis on the local balance of the vertically integrated kinetic energy in the time mean flow and transient eddies was performed by Holopainen (1978). His work made use of annual mean circulation statistics derived from station data for the years 1950–54 and 1958–62. The results of that study also indicate the importance of the divergence fields of horizontal transports by the time mean flow. The geographical locations of the principal sources and sinks of $\bar{K}_M$ and $\bar{K}_T$, as inferred from our results, are in agreement with the findings of Holopainen's study.

7. Discussion

A recent modeling study by Simmons and Hoskins (1978) on the temporal evolution of nonlinear transient waves on a sphere demonstrates that these disturbances are characterized by well-defined life cycles. Synoptic-scale perturbations superimposed on a balanced zonal mean flow are seen to grow initially by baroclinic instability, with vigorous generation of kinetic energy through strong temperature advection in the vertical and meridional directions. After about eight days of model integration, these disturbances reach the occluded stage and thereafter they gradually acquire a barotropic character, with much weakened heat fluxes. The momentum fluxes in this decaying phase generally result in the transfer of kinetic energy from the transient eddies to the mean flow, so that the disturbances eventually dissipate at a rate similar to their earlier baroclinic growth. Some of the characteristics of the occluding disturbances were also noted by Gall (1976) as he followed the growth of baroclinic waves into the nonlinear regime.

The regional character of the circulation statistics presented in B, L and the present paper is in qualitative agreement with the behavior of the modeled nonlinear baroclinic-barotropic waves at different stages of their life cycle. In the real atmosphere, the kinetic energy of the locally intense time mean flow over eastern Asia and eastern North America is maintained by the time-averaged, thermally direct meridional circulations at these longitudes, as shown in Fig. 8. These regions are characterized by strong wind shears and baroclinity and hence are favored sites for the initiation of traveling baroclinic cyclones (Petterssen, 1956; Reitan, 1974). During the growth phase of these disturbances, they extract energy from the time mean flow by transporting heat poleward and upward. These waves propagate eastward with a typical phase speed of about 10° longitude per day and a growth period of several days, so that maximum amplitude is attained over the mid-oceans. The vertical structure of the phase relations (Figs. 5 and 6) and amplitude (L, Figs. 4–7) of the disturbances over these oceanic storm tracks bear a distinct resemblance to that obtained by Simmons and Hoskins (1977) for linearly growing modes. As these disturbances move still further eastward and reach the western continents, the wave tilt in the vertical direction decreases (Fig. 5), the poleward and upward heat transports are much weakened, and barotropic processes dominate the local energetics. The tendency for the momentum transports over the western United States and western Europe (Lau *et al.*, 1978, Fig. 1) to impart westerly momentum to the mean flow is counteracted by the prevalence of the time-averaged, thermally indirect meridional circulations in these meridional sectors, which act to destroy $\bar{K}_M$ (Fig. 8). As has been demonstrated in the previous section, the dissipation of both $\bar{K}_M$ and $\bar{K}_T$ over the western continents is locally compensated by the mean flow advection of kinetic energy from upstream.

The basic assumption underlying the above comparisons between the observational and modeling results is that all disturbances form near the east coasts of Asia and North America, and evolve through their life cycles at the same rate as they move along well-defined storm tracks across the midlatitude oceans, which end in the decay regions over the western continents. Since the transient disturbances that exist in nature do depart from this idealized situation, the contrast between the growing and decaying stages inferred from the present study may be smeared out to a certain extent. A better comparison between observation and theory may be achieved by compositing suitably selected disturbances appearing in the NMC data set according to the phase of these waves relative to their individual life cycles, and by categorizing these waves according to their spatial and temporal scales.

Acknowledgments. I wish to thank Professor John M. Wallace for his guidance throughout the course of this study. I am also indebted to Dr. Maurice L. Blackmon for his support of this work, to Dr. Yoshikazu Hayashi and other staff members of the Geophysical Fluid Dynamics Laboratory for many helpful discussions, and to Mr. Roy Jenne and his associates for making the NMC data set available. The comments by the official reviewers led to several clarifications of the manuscript.

This work was jointly supported by the National Science Foundation under Grant ATM 78-07369 (Climate Dynamics Program, Climate Dynamics

Research Section), and by a National Center for Atmospheric Research graduate assistantship. Acknowledgment is made to the NCAR Computer Facility for extensive use of its resources, and to Messrs. John Conner, William Ellis and Philip Tunison of the Geophysical Fluid Dynamics Laboratory for their assistance in drafting some of the figures.

REFERENCES

Amos, D. E., and L. H. Koopmans, 1963: Tables of the distribution of the coefficient of coherence for stationary bivariate Gaussian processes. Memo. SCR-483, Sandia Corp., Albuquerque, N.M., 328 pp.

Blackmon, M. L., 1976: A climatological spectral study of the 500 mb geopotential height of the Northern Hemisphere. *J. Atmos. Sci.*, **33**, 1607–1623.

——, J. M. Wallace, N-C. Lau and S. L. Mullen, 1977: An observational study of the Northern Hemisphere wintertime circulation. *J. Atmos. Sci.*, **34**, 1040–1053.

Gall, R., 1976: Structural changes of growing baroclinic waves. *J. Atmos. Sci.*, **33**, 374–390.

Hartmann, D. L., 1974: Time spectral analysis of mid-latitude disturbances. *Mon. Wea. Rev.*, **102**, 348–362.

Holopainen, E., 1978: A diagnostic study of the kinetic energy balance of the long-term mean flow and the associated transient fluctuations in the atmosphere. *Geophysica*, **15**, 125–145.

Jensen, C. E., 1961: Energy transformation and vertical flux processes over the Northern Hemisphere. *J. Geophys. Res.*, **66**, 1145–1156.

Lau, N-C., 1978: On the three-dimensional structure of the observed transient eddy statistics of the Northern Hemisphere wintertime circulation. *J. Atmos. Sci.*, **35**, 1900–1923.

——, H. Tennekes and J. M. Wallace, 1978: Maintenance of the momentum flux by the transient eddies in the upper troposphere. *J. Atmos. Sci.*, **35**, 139–147.

Manabe, S., and J. L. Holloway, Jr., 1975: The seasonal variations of the hydrologic cycle as simulated by a global model of the atmosphere. *J. Geophys. Res.*, **80**, 1617–1649.

Molla, A. C., Jr., and C. J. Loisel, 1962: On the hemispheric correlation of vertical and meridional wind components. *Geofis. Pura Appl.*, **51**, 166–170.

Möller, F., 1951: Quarterly charts of rainfall for the whole earth. *Petermanns Geogr. Mitt.*, **95**, 1–7.

Namias, J., and P. F. Clapp, 1949: Confluence theory of high tropospheric jet stream. *J. Meteor*, **6**, 330–336.

Oort, A. H., and P. H. Chan, 1977: On the role of the Asian monsoon in the angular momentum and kinetic energy balances of the tropics. *Pure Appl. Geophys.*, **115**, 1167–1186.

——, and J. P. Peixóto, 1974: The annual cycle of the energetics of the atmosphere on a planetary scale. *J. Geophys. Res.*, **79**, 2705–2719.

Petterssen, S., 1956: *Weather Analysis and Forecasting*, Vol. 1. McGraw Hill, 267–276.

Pratt, R. W., and J. M. Wallace, 1976: Zonal propagation characteristics of large-scale fluctuations in the mid-latitude troposphere. *J. Atmos. Sci.*, **33**, 1184–1194.

Reitan, C. H., 1974: Frequencies of cyclones and cyclogenesis for North America, 1951–1970. *Mon. Wea. Rev.*, **102**, 861–868.

Shuman, F. G., and J. Hovermale, 1968: An operational six-layer primitive equation model. *J. Appl. Meteor.*, **7**, 525–547.

Simmons, A. J., and B. J. Hoskins, 1977: Baroclinic instability on the sphere: Solution with a more realistic tropopause. *J. Atmos. Sci.*, **34**, 581–588.

——, and ——, 1978: The life cycles of some nonlinear baroclinic waves. *J. Atmos. Sci.*, **35**, 414–432.

U.S. Dept. of Commerce and U.S. Air Force, 1971: *Global Atlas of Relative Cloud Cover 1967–70*, p. 106. [Available from Director, National Climatic Center, Asheville, NC 28801].

Wallace, J. M. and P. V. Hobbs, 1977: *Atmospheric Science: An Introductory Survey*. Academic Press, 467 pp.

Wiin-Nielsen, A., 1959: A study of energy conversion and meridional circulation for the large-scale motion in the atmosphere. *Mon. Wea. Rev.*, **87**, 319–332.

——, 1964: On energy conversion calculations. *Mon. Wea. Rev.*, **92**, 161–167.